J|A|C|S ARTICLES

Published on Web 06/15/2009

One-Pot Synthesis of Platinum-Based Nanoparticles Incorporated into Mesoporous Niobium Oxide−Carbon Composites for Fuel Cell Electrodes

M. Christopher Orilall,[†,‡] Futoshi Matsumoto,[†] Qin Zhou,[†] Hiroaki Sai,[‡] Héctor D. Abruña,[†] Francis J. DiSalvo,[†] and Ulrich Wiesner*[,‡]

Department of Chemistry and Chemical Biology and Department of Materials Science and Engineering, Cornell University, Ithaca, New York 14853

Received April 23, 2009; E-mail: ubw1@cornell.edu

Abstract: Catalyst-electrode design is crucial for the commercialization and widespread use of polymer electrolyte membrane fuel cells. There are considerable challenges in making less expensive, more durable, and more active catalysts. Herein, we report the one-pot synthesis of Pt and Pt−Pb nanoparticles incorporated into the pores of mesoporous niobium oxide−carbon composites. The self-assembly of block copolymers with niobium oxide and metal precursors results in an ordered mesostructured hybrid. Appropriate heat treatment of this hybrid produces highly crystalline, well-ordered mesoporous niobium oxide−carbon composites with Pt (or Pt−Pb) nanoparticles incorporated into the mesopores. The in situ-generated graphitic-like carbon material prevents the collapse of the mesostructure, while the metal oxide crystallizes at high temperatures and enhances the electrical conductivity of the final material. Formic acid electrooxidation with this novel material shows 4 times higher mass activities (3.3 mA/μg) and somewhat lower onset potentials (−0.24 V vs Ag/AgCl) than the best previously reported values employing Pt−Pb intermetallic nanoparticles supported on conducting carbon (0.85 mA/μg and −0.18 V, respectively).

Introduction

Fuel cells offer a promising concept for a clean and efficient means of energy conversion. Direct fuel cells use liquid fuels without a reforming step. Formic acid (FA) as a fuel has gained special interest recently because of good power densities due to low oxidation overpotentials at reasonable current densities and its much lower crossover rate through the polymer membrane compared with methanol.[1] Materials limitations in current fuel-cell technology prevent large-scale commercialization. Among these, durability and degradation issues are particularly prominent.[2,3] Besides the polymer membrane, catalyst-electrode design is an area where materials innovations are expected to be important. Current polymer electrolyte membrane fuel cell (PEMFC) technology employs a heterogeneous mixture of Pt nanoparticles dispersed on high-surface-area carbon supports. This design leads to limitations such as mass-transport and Ohmic resistance. Moreover, the electrochemical oxidation of carbon leads to electrode degradation[4−6] and thus reduces the lifetime of PEMFCs. Additionally, Pt has been shown to accelerate this carbon corrosion.[7] Therefore, alternative choices of electrode materials are being considered.

Transition-metal oxides are promising candidates for the electrocatalyst support. Materials such as Nb_2O_5, TiO_2, and WO_3 are stable under fuel-cell conditions (i.e., low pH and applied potentials relevant to PEMFCs[8]) but are insulators. Previous studies have reported work on WO_3,[9−11] TiO_2,[12] conducting phases of TiO_{2-x},[13−15] and other oxides such as SnO_2,[16] RuO_2,[17] MoO_x,[18] IrO_2,[19] and indium tin oxide.[20] Results to date have indicated that transition-metal oxides can enhance the electro-

[†] Department of Chemistry and Chemical Biology.
[‡] Department of Materials Science and Engineering.

(1) Qian, W.; Wilkinson, D. P.; Shen, J.; Wang, H.; Zhang, J. *J. Power Sources* **2006**, *154*, 202–213.
(2) Borup, R.; et al. *Chem. Rev* **2007**, *107*, 3904–3951.
(3) Shao, Y.; Yin, G.; Gao, Y. *J. Power Sources* **2007**, *171*, 558–566.
(4) Gallagher, K. G.; Wong, D. T.; Fuller, T. F. *J. Electrochem. Soc.* **2008**, *155*, B488–B493.
(5) Meyers, J. P.; Darling, R. M. *J. Electrochem. Soc.* **2006**, *153*, A1432–A1442.
(6) Stevens, D. A.; Dahn, J. R. *Carbon* **2005**, *43*, 179–188.
(7) Roen, L. M.; Paik, C. H.; Jarvi, T. D. *Electrochem. Solid-State Lett.* **2004**, *7*, A19–A22.
(8) Pourbaix, M. *Atlas of Electrochemical Equilibria in Aqueous Solutions*; NACE International: Houston, TX, 1974.
(9) Ganesan, R.; Lee, J. S. *J. Power Sources* **2006**, *157*, 217–221.
(10) Jayaraman, S.; Jaramillo, T. F.; Baeck, S. H.; McFarland, E. W. *J. Phys. Chem. B* **2005**, *109*, 22958–22966.
(11) Cui, X.; Shi, J.; Chen, H.; Zhang, L.; Guo, L.; Gao, J.; Li, J. *J. Phys. Chem. B* **2008**, *112*, 12024–12031.
(12) Gustavsson, M.; Ekstroem, H.; Hanarp, P.; Eurenius, L.; Lindbergh, G.; Olsson, E.; Kasemo, B. *J. Power Sources* **2007**, *163*, 671–678.
(13) Chen, G.; Bare, S. R.; Mallouk, T. E. *J. Electrochem. Soc.* **2002**, *149*, A1092–A1099.
(14) Garcia, B. L.; Fuentes, R.; Weidner, J. W. *Electrochem. Solid-State Lett.* **2007**, *10*, B108–B110.
(15) Raghuveer, V.; Viswanathan, B. *J. Power Sources* **2005**, *144*, 1–10.
(16) Saha, M. S.; Li, R.; Cai, M.; Sun, X. *Electrochem. Solid-State Lett.* **2007**, *10*, B130–B133.
(17) Gu, Y.-J.; Wong, W.-T. *J. Electrochem. Soc.* **2006**, *153*, A1714–A1718.
(18) Ioroi, T.; Yasuda, K.; Siroma, Z.; Fujiwara, N.; Miyazaki, Y. *J. Electrochem. Soc.* **2003**, *150*, A1225–A1230.
(19) Chen, A.; LaRussa, D. J.; Miller, B. *Langmuir* **2004**, *20*, 9695–9702.
(20) Chhina, H.; Campbell, S.; Kesler, O. *J. Power Sources* **2006**, *161*, 893–900.

Scheme 1. Schematic Representation of the Demonstrated One-Pot Method[a]

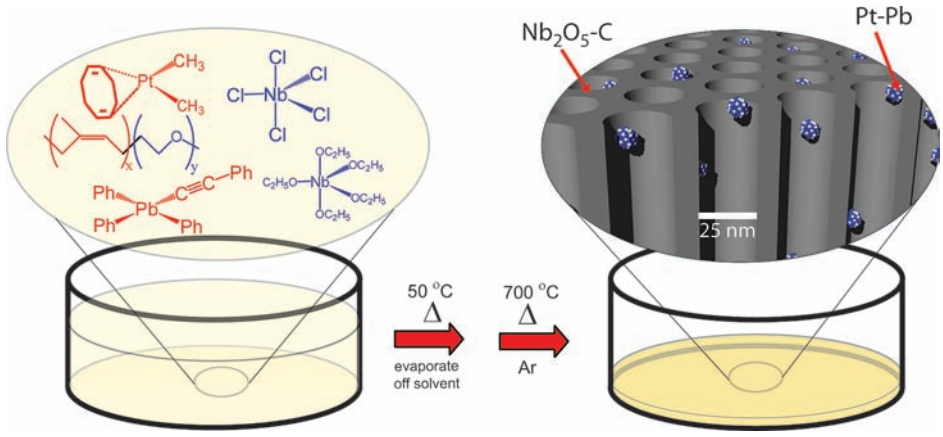

[a] Niobium oxide, Pt, and Pb precursors are structure-directed by poly(isoprene-*block*-ethylene oxide) (PI-*b*-PEO) to give a highly crystalline mesoporous Nb_2O_5−C structure with Pt−Pb nanoparticles inside the mesopores after heat treatment at high temperatures under an inert environment.

catalytic activity[12] and minimize the poisoning from carbon monoxide (CO) in methanol fuel cells.[21] However, most of these materials systems are not highly porous, and the electrocatalysts have mainly been dispersed on conducting carbon. It is well-established that highly porous, nanostructured electrodes, once fabricated, would maximize reaction surface area and optimize performance[22] and are thus desirable. In particular, highly porous niobium oxide (Nb_2O_5 or NbO_2) would be very interesting because of its known strong metal−support interaction (SMSI) effects.[23,24]

Herein, we report the one-pot synthesis of Pt- and Pt−Pb-based nanoparticles incorporated into the pores of mesoporous niobium dioxide−carbon composites (Nb_2O_5−C and NbO_2−C). In situ-generated carbon (∼15 wt %) was produced, helping to prevent the collapse of the mesostructure, while the amorphous oxide was crystallized at high temperatures. This system was tested for potential use as an anode material through the electrooxidation of formic acid. It shows mass activities as high as 4 times the best previously reported value for intermetallic Pt−Pb nanoparticles supported on conducting carbon, with an onset potential for FA oxidation that is 60 mV less positive. At the same time, this composite shows enhanced tolerance toward poisoning by CO. While this material does not completely overcome the issue of carbon degradation, it represents a step in the right direction and paves the way for the development of more stable electrocatalyst support systems.

Our approach utilizes a combined assembly by soft and hard (CASH) chemistry.[25] Nanostructure control is achieved by using the thermodynamically controlled phase-separation phenomena observed for block copolymers.[26,27] Here, a diblock copolymer, poly(isoprene-*block*-ethylene oxide) (PI-*b*-PEO), is used to simultaneously structure-direct niobium oxide sols and Pt (and Pb) precursor(s) of the catalyst nanoparticles.[28] The niobium oxide sol mixes with the PEO block of the copolymer.[29] Self-assembly leads to a hexagonally arranged cylindrical morphology with an oxide/PEO matrix. The Pt (and Pb) precursor(s) mix(es) with the PI block to form the cylinders. Heat treatment of this amorphous organic−inorganic nanostructured hybrid material under flowing inert gas (N_2 or Ar) at high temperatures (>500 °C) simultaneously removes the PEO components of the hybrid, reduces the metal precursors to nanoparticles, carbonizes the PI components,[25] and converts the amorphous metal oxide to highly crystalline Nb_2O_5 while transforming the material into a mesoporous structure (see Scheme 1). The carbonization of the PI enables high-temperature treatments without collapse of the nanostructure.[25] Characterization data from transmission electron microscopy (TEM), scanning electron microscopy (SEM), small-angle X-ray scattering (SAXS), powder X-ray diffraction (XRD), Brunauer−Emmett−Teller (BET) surface area analysis, X-ray photoelectron spectroscopy (XPS), thermogravimetric analysis (TGA), energy dispersive X-ray (EDAX) microanalysis, and Raman spectroscopy will be presented along with electrochemical data for FA oxidation with these materials in order to investigate their compositional and structural evolution and functionality.

Experimental Section

The polymer used was PI-*b*-PEO with $M_n = 33.5$ kg mol^{-1} and 23 wt % PEO. Anionic polymerization techniques were employed, resulting in a low molecular weight distribution with a corresponding polydispersity index of 1.02.[30,31] The following is a typical procedure for the synthesis of 5 wt % Pt nanoparticle-loaded mesoporous niobium dioxide: In a glovebox, 0.1 g of $NbCl_5$ (Sigma-Aldrich) followed by 0.15 mL of $Nb(OEt)_5$ (Sigma-Aldrich) was added to a solution of the polymer (0.075 g), which was dissolved in anhydrous chloroform[32,33] and allowed to stir for 12 h. Platinum

(21) Uribe, F. A.; Valerio, J. A.; Garzon, F. H.; Zawodzinski, T. A. *Electrochem. Solid-State Lett.* **2004**, *7*, A376–A379.
(22) O'Hayre, R.; Cha, S. W.; Colella, W.; Prinz, F. B. *Fuel Cell Fundamentals*; John Wiley & Sons: Hoboken, NJ, 2005.
(23) Sasaki, K.; Zhang, L.; Adzic, R. R. *Phys. Chem. Chem. Phys.* **2008**, *10*, 159–167.
(24) Krstajic, N. V.; Vracar, L. M.; Neophytides, S. G.; Jaksic, J. M.; Murase, K.; Tunold, R.; Jaksic, M. M. *J. New Mater. Electrochem. Syst.* **2006**, *9*, 83–97.
(25) Lee, J.; Orilall, M. C.; Warren, S. C.; Kamperman, M.; DiSalvo, F. J.; Wiesner, U. *Nat. Mater.* **2008**, *7*, 222–228.
(26) Cho, B. K.; Jain, A.; Gruner, S. M.; Wiesner, U. *Science* **2004**, *305*, 1598–1601.
(27) Hamley, I. W. *The Physics of Block Copolymers*; Oxford University Press: New York, 1998.
(28) Templin, M.; Franck, A.; Du Chesne, A.; Leist, H.; Zhang, Y.; Ulrich, R.; Schadler, V.; Wiesner, U. *Science* **1997**, *278*, 1795–1798.
(29) Warren, S. C.; DiSalvo, F. J.; Wiesner, U. *Nat. Mater.* **2007**, *6*, 156–161.
(30) Hsieh, H. L.; Quirk, R. P. *Anionic Polymerization: Principles and Practical Applications*; Marcel Dekker: New York, 1996.
(31) Allgaier, J.; Poppe, A.; Willner, L.; Richter, D. *Macromolecules* **1997**, *30*, 1582–1586.
(32) Acosta, S.; Corriu, R.; Leclercq, D.; Mutin, P. H.; Vioux, A. *J. Sol-Gel Sci. Technol.* **1994**, *2*, 25–28.

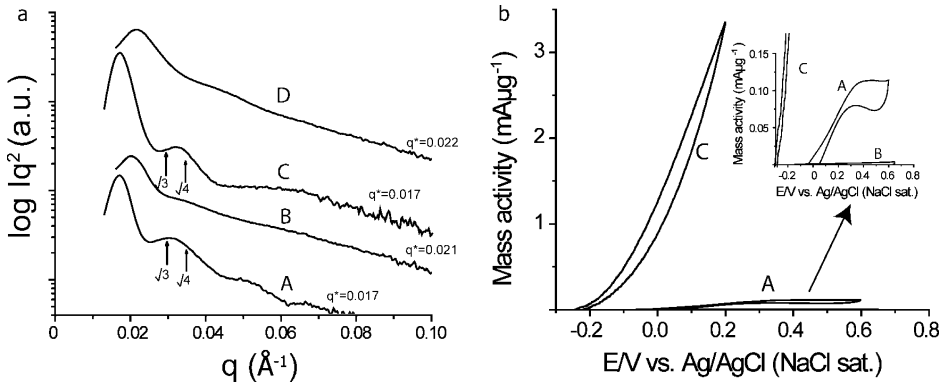

Figure 1. Materials characterization by SAXS and electrochemical oxidation of FA. (a) SAXS traces for (A) as-made composite CCM-Nb_2O_5-C-Pt, (B) crystalline CCM-Nb_2O_5-C-Pt, (C) as-made CCM-Nb_2O_5-C-Pt-Pb composite, and (D) crystalline CCM-Nb_2O_5-C-Pt-Pb. (b) Rotating-disk-electrode voltammograms for FA oxidation in an aqueous solution containing 0.5 M FA and 0.1 M H_2SO_4 at 10 mV/s and 2000 rpm using (A) CCM-NbO_2-C-Pt and (C) CCM-NbO_2-C-Pt-Pb. Voltammogram B was obtained using 0.1 M H_2SO_4 solution without FA under the same conditions as for A and C (the inset zooms in on A and B).

dimethylcyclooctadiene (0.013 g) was added to the mixture, which was stirred for 10 min. For Pt−Pb-based materials, 0.018 g of triphenyl(phenylethynyl)lead (Sigma-Aldrich) was added after addition of the platinum precursor to give a total metal loading of 10 wt %. Films were cast by evaporation of the solvent and byproducts in air on a hot plate at 50 °C. The as-synthesized amorphous material was heat-treated in a flow-through furnace to 700 °C using a 1 °C/min ramp for 2 h under argon to produce a crystalline Nb_2O_5−C composite. The resulting material was subsequently heated to 875 °C at a rate of 1 °C/min for 2 h under forming gas to reduce Nb_2O_5 to NbO_2.

The electrocatalytic activities of the materials toward FA oxidation were examined. Prior to each experiment, a suspension of the nanoparticle catalyst was prepared as follows: To 8 mg of the dried sample (e.g., CCM-NbO_2-C-Pt-Pb), 3.98 mL of distilled water and 1 mL of isopropyl alcohol (Aldrich) were added. Additionally, 20 μL of a 5% (w/w) Nafion solution in alcohols (Aldrich, EW 1100) and water were added to this mixture. The resulting mixture was sonicated in a bath-type ultrasonicator for 15 min. The nanoparticle suspension described above was coated onto a 3 mm diameter glassy carbon (GC) electrode. The electrode had been previously polished with diamond paste (METADI-Buehler, ø = 1 μm) and ultrasonicated in Millipore water (18 MΩ/cm, Millipore Milli-Q) for 10 min. The electrode was then rinsed with Millipore water and allowed to dry in air, after which the sample was coated (140 μg/cm^2) onto the clean glassy carbon electrode. The catalyst loading for a 5 wt % Pt sample (e.g., CCM-NbO_2-C-Pt) was therefore calculated as 7 μg/cm ^{2}, and this value was used for mass activity calculations. The electrode was then spin-dried at 600 rpm under a nitrogen gas atmosphere. Before the investigation of fuel oxidation, an electrochemical pretreatment of the nanoparticle-coated electrodes was preformed. For CCM-NbO_2-C-Pt samples, the literature procedure of cycling the nanoparticle-coated electrodes between −0.3 and 1.4 V for 10 cycles at 10 mV/s in 0.1 M H_2SO_4 (J. T. Baker ultrapure reagent) was employed to activate the catalyst surface, presumably by removing some contaminants.[34] For CCM-NbO_2-C-Pt-Pb and Pt−Pb on Vulcan samples, a partially optimized procedure involved generating hydrogen by holding the nanoparticle electrodes at −0.7 V for 30 min in 0.1 M H_2SO_4 to activate the nanoparticle surfaces. FA oxidation on the nanoparticle-coated GC electrode was examined in a mixture of 0.5 M FA (Mallinckrodt, 88% analytical reagent) and 0.1 M H_2SO_4 at a sweep rate of 10 mV/s. All of the solutions were prepared with Millipore water and deaerated with prepurified nitrogen for at least 10 min before each experiment. The measurements were conducted at room temperature. All potentials are referenced to a sodium chloride-saturated Ag/AgCl electrode without regard for the liquid junction.

SAXS experiments were performed on the G1 station at CHESS and on a Rigaku RU-H3R copper rotating anode (λ = 1.54 Å). XRD data were obtained from powdered samples using a Scintag Inc. q-q diffractometer (Cu Kα, 1.54 Å). TEM on a FEI Tecnai T12 transmission electron microscope at 120 kV was used to capture the images in Figure 2. Nitrogen adsorption/desorption isotherms were measured at −196 °C using a Micromeritics ASAP 2020 system. The samples were degassed at 120 °C overnight. Raman data was collected on a Renishaw InVia microRaman system. TGA was performed on a TG/DTA 320 instrument using a heating rate of 5 °C/min. XPS was carried out using a Surface Science Instruments SSX-100 UHV system.

Results and Discussion

In the demonstrated one-pot approach, the niobium oxide sol precursors (niobium chloride and niobium ethoxide) are first added to a chloroform solution of the block copolymer PI-*b*-PEO with a molecular weight of 33.5 kg/mol and PEO content of 23 wt %. The solution is stirred overnight to allow the niobium oxide nonhydrolytic sol−gel reaction to proceed.[35] The platinum precursor (platinum dimethylcyclooctadiene) is then added and the solution stirred for 10 min. Heating this solution at 50 °C in air and allowing the volatiles to evaporate results in a well-ordered amorphous organic−inorganic hybrid material (as-made CCM-Nb_2O_5-C-Pt). The metal oxide sol particles selectively swell the PEO block,[25] while the hydrophobic platinum precursor is expected to preferentially mix with the PI block. Structure characterization of this as-made material was performed by SAXS. A representative diffractogram of the material (Figure 1a, trace A) shows a first-order peak centered around a value of the scattering wavevector, q ($q = 4\pi \sin\theta/\lambda$, where 2θ is the scattering angle and λ is the X-ray wavelength), corresponding to a d spacing of 36.9 nm along with at least one broad higher-order peak. In Figure 1a, ticks indicate the expected angular positions of $\sqrt{3}$ and $\sqrt{4}$ of the first-order maximum expected for a hexagonally ordered structure with cylinders consisting of PI and the platinum molecular precursor inside a matrix of PEO and amorphous Nb_2O_5. This proposed

(33) Tian, B.; Liu, X.; Tu, B.; Yu, C.; Fan, J.; Wang, L.; Xie, S.; Stucky, G. D.; Zhao, D. *Nat. Mater.* **2003**, *2*, 159–163.
(34) Volpe, D.; Casado-Rivera, E.; Alden, L.; Lind, C.; Hagerdon, K.; Downie, C.; Korzeniewski, C.; DiSalvo, F. J.; Abruna, H. D. *J. Electrochem. Soc.* **2004**, *151*, A971–A977.
(35) Arnal, P.; Corriu, R. J. P.; Leclercq, D.; Mutin, P. H.; Vioux, A. *Mater. Res. Soc. Symp. Proc.* **1994**, *346*, 339–344.

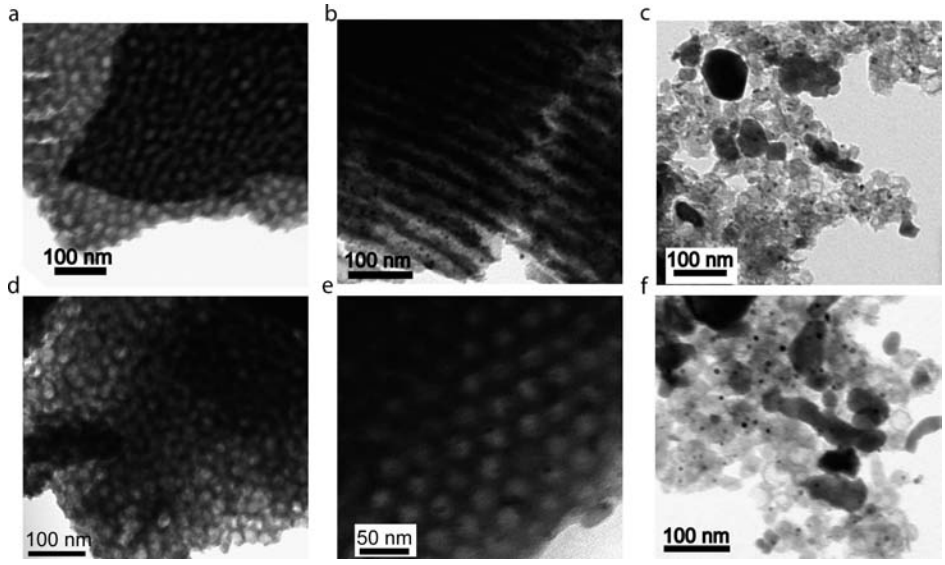

Figure 2. Materials characterization by TEM: (a) as-made composite CCM-Nb_2O_5-C-Pt; (b) crystalline CCM-Nb_2O_5-C-Pt; (c) crystalline CCM-NbO_2-C-Pt; (d) as-made composite CCM-Nb_2O_5-C-Pt-Pb; (e) crystalline CCM-Nb_2O_5-C-Pt-Pb; (f) crystalline CCM-NbO_2-C-Pt-Pb.

structure is supported by TEM imaging of various local sections of the as-made material (Figure 2a).

Heat treatment of this hybrid to 700 °C under a flowing inert gas simultaneously converts the amorphous Nb_2O_5 into highly crystalline Nb_2O_5, burns off the PEO, transforms the PI to an amorphous graphitic-like carbon material lining the pore walls,[25] and reduces the platinum precursor to platinum nanoparticles. Because the platinum precursor preferentially resides in the PI domains, the resulting structure should now have the platinum nanoparticles mainly decorating the pore walls (CCM-Nb_2O_5-C-Pt). SAXS characterization of this material is indicative of some degree of long-range order. Diffractograms of CCM-Nb_2O_5-C-Pt show a first-order peak with corresponding d spacing of 29.9 nm and a weak, broad second-order peak (Figure 1a, trace B). Peaks are shifted to larger q values with respect to the as-made composite because of shrinkage upon removal of the organics. TEM imaging of various sections of the material shows pores with an average diameter of 24 nm and Pt particles with an average size of 8 nm inside these pores (Figure 2b). XRD patterns and their analysis reveal sharp reflections for the material corresponding to crystalline Nb_2O_5 (PDF no. 1007-433) as well as broad peaks corresponding to Pt (PDF no. 812-9818) (Figure 3a). The domain size of the Pt nanoparticles, as calculated using the Debye−Scherer formula on the [111] reflection peak, is 10 ± 2 nm, consistent with the TEM imaging results. The average domain size of the Nb_2O_5 crystallites is 30 ± 4 nm as estimated from the [001] and [002] reflections and 12 ± 2 nm for all other reflections, consistent with previous studies on similarly prepared nonfunctionalized mesoporous Nb_2O_5.[25] This result suggests that the Nb_2O_5 grains are elongated along the (001) direction. The mesoporous nature of the material is confirmed by nitrogen physisorption data, which show a type-IV nitrogen sorption isotherm (Figure 4a, trace A) with a specific surface area of 145.3 m^2/g and a uniform pore size distribution centered around 29 nm as obtained from Barrett−Joyner−Halenda (BJH) analysis (see Figure 4a inset, trace A), in good agreement with the TEM results.

A fraction of the surface area was estimated by BET modeling to be microporous surface area. We expect that this arises from the small amount of in situ-generated carbon[25] that is still present in the material [∼15% by weight as suggested by TGA; the presence of carbon was confirmed by Raman spectroscopy (Figures S1 and S2, respectively, in the Supporting Information)]. While this nanostructured material has a high surface area and should provide good accessibility of fuel to the catalyst, its use in fuel-cell applications may be limited since Nb_2O_5 is an insulator. It should be noted, however, that the carbon provides some conductivity.

An alternate way to increase conductivity is to reduce Nb_2O_5 to NbO_2, which is a semiconductor.[36] To this end, we heat-treated CCM-Nb_2O_5-C-Pt under forming gas for 2 h at 875 °C. This resulted in Pt nanoparticles supported by highly crystalline mesoporous NbO_2 (CCM-NbO_2-C-Pt). The crystalline phase of the material was confirmed by XRD experiments (Figure 3b), which showed sharp reflections corresponding to crystalline NbO_2 (PDF no. 04-005-4298) and broader peaks corresponding to Pt (PDF no. 812-9818). The average domain size of the NbO_2 crystallites as calculated using the Debye−Scherer equation is 80 ± 5 nm, while that for the Pt nanoparticles is 10 ± 2 nm using the [111] reflection. As a result of the large growth of the NbO_2 crystallites relative to the Nb_2O_5 ones, there is a significant loss of order of the mesopores of the parent material. Nonetheless, the mesoporous nature of the material is retained, as confirmed by nitrogen physisorption data showing a type-IV nitrogen sorption isotherm (Figure 4a, trace B) with a specific surface area of 136.55 m^2/g and a uniform pore size distribution centered around 28 nm (Figure 4a inset, trace B). This was corroborated by TEM imaging of the material, which showed nanoparticles uniformly dispersed on a porous matrix (Figure 2c). TGA and Raman spectroscopy of this material confirmed that the 15 wt % in situ-generated carbon is still present (Figures S3 and S4, respectively, in the Supporting Information).

Trace A in Figure 1b shows the rotating-disk-electrode voltammogram for FA oxidation using CCM-NbO_2-C-Pt. For an aqueous solution containing 0.5 M FA and 0.1 M H_2SO_4, CCM-NbO_2-C-Pt with a total Pt loading of 2 wt % exhibited an onset potential of −0.041 V and a mass activity of 0.069 mA/μg. The mass activity (in mA/μg) was here defined as the oxidation current at 0.2 V normalized to the loading (wt %) of

(36) Roberson, J. A.; Rapp, R. A. *J. Phys. Chem. Solids* **1969**, *30*, 1119–1124.

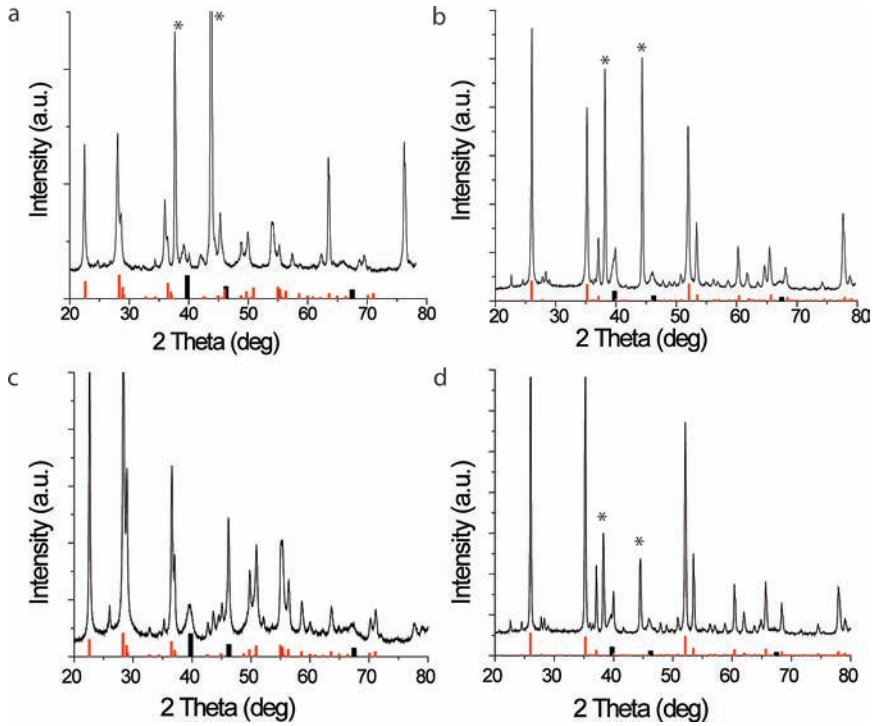

Figure 3. Materials characterization by powder XRD: (a) CCM-Nb_2O_5-C-Pt; (b) CCM-NbO_2-C-Pt; (c) CCM-Nb_2O_5-C-Pt-Pb; (d) CCM-NbO_2-C-Pt-Pb. Light bar markers signify the peaks expected for the crystalline Nb_2O_5 structure (PDF no. 1007-433) or crystalline NbO_2 structure (PDF no. 04-005-4298), while dark bar markers signify the peaks expected for the crystalline Pt structure (PDF no. 812-9818). Asterisks indicate peaks corresponding to the sample holder.

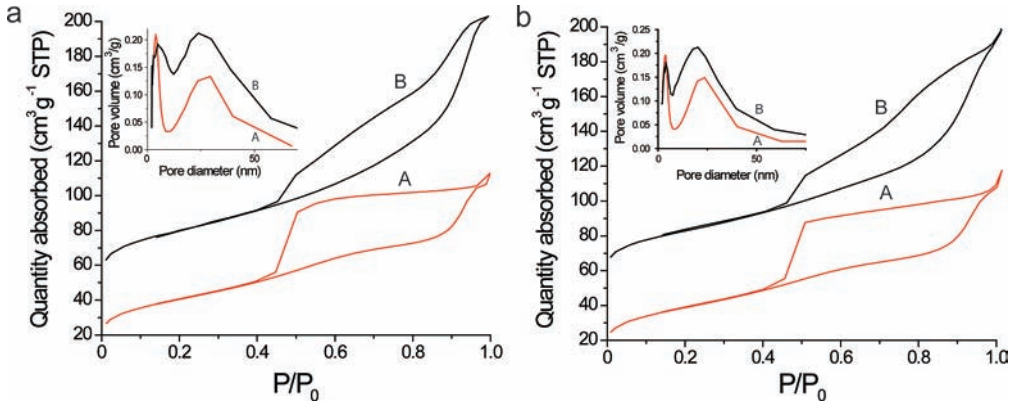

Figure 4. Materials characterization by nitrogen physisorption. (a) Nitrogen adsorption−desorption isotherms for (A) CCM-Nb_2O_5-C-Pt and (b) CCM-NbO_2-C-Pt. The inset shows the corresponding pore size distributions. (b) Nitrogen adsorption−desorption isotherms of (A) CCM-Nb_2O_5-C-Pt-Pb and (B) CCM-NbO_2-C-Pt-Pb. The inset shows the corresponding pore size distributions. Pore size distributions were calculated by the BJH method using the adsorption isotherm. The data are offset by 20% along the *y* axis for B in both the isotherms and the pore size distributions.

the metal nanoparticle (electrocatalyst) (in this case Pt). We defined the onset potential as the point at which the mass activity reached 0.005 mA/μg. CCM-NbO_2-C-Pt did not show any redox response in a solution containing only 0.1 M H_2SO_4 (other than the double-layer charging processes) over the potential range examined (Figure 1b, trace B). For CCM-NbO_2-C-Pt, the onset potential was slightly less negative and the mass activity was larger compared with CCM-Nb_2O_5-C-Pt at a similar catalyst loading (Table 1). This simple one-pot approach for making Pt nanoparticles incorporated into mesoporous and crystalline NbO_2 allows for higher Pt loadings by merely increasing the initial amount of Pt precursor. Table 1 shows a summary of FA oxidation for CCM-NbO_2-C-Pt electrodes with catalyst loadings of 2, 5, and 10 wt %. The mass activities and onset potentials of these electrodes are comparable to those of carbon-supported Pt nanoparticles.

Table 1. Comparison of the Mass Activities and Onset Potentials for FA Oxidation Using Different Materials at Various Catalyst Loadings (i.e., wt % Pt or Pt−Pb)

sample	total loading (wt %)	surface area (m^2/g)	micropore area (m^2/g)	onset potential (V)	mass activity (mA/μg) at 0.2 V
Nb_2O_5-C-Pt	2	145.3	62.33	−0.016	0.020
NbO_2-C-Pt	2	136.6	54.35	−0.041	0.069
NbO_2-C-Pt	5	200.9	72.21	−0.097	0.076
NbO_2-C-Pt	10	216.9	43.28	−0.017	0.033
Nb_2O_5-C-Pt-Pb	5	171.5	60.90	−0.177	0.149
NbO_2-C-Pt-Pb	5	175.2	60.54	−0.243	3.349
NbO_2-C-Pt-Pb	10	196.2	57.18	−0.194	0.723
NbO_2-C-Pt-Pb	20	149.5	57.72	−0.194	0.789

In an attempt to achieve higher mass activities and lower onset potentials, we attempted to prepare Pt−Pb intermetallic nanoparticles inside the mesopores of the niobium oxide structure. It has previously been shown that Pt−Pb intermetallic nanoparticles supported on conducting carbon exhibit high mass activity and low onset potential toward FA oxidation.[37−39] In order to keep the synthesis a simple one-pot approach, we simply added an equimolar amount of lead and platinum precursors to the block copolymer−metal oxide solution. This resulted in an ordered mesostructured organic−inorganic hybrid (as-made CCM-Nb_2O_5-C-Pt-Pb). SAXS analysis of the material (see Figure 1a, trace C) showed a first-order peak centered around a q value corresponding to a d spacing of 36.9 nm along with at least one broad second-order peak. The order of the mesostructure was confirmed by TEM imaging of various local sections of the as-made material (Figure 2d). To obtain a highly crystalline, mesoporous material, as-made hybrids were heat-treated at 700 °C under Ar. The resulting materials (CCM-Nb_2O_5-C-Pt-Pb) showed that the mesostructure was maintained. The SAXS diffractogram of CCM-Nb_2O_5-C-Pt-Pb exhibits a first-order peak with corresponding d spacing of 28.5 nm and a weak, broad second-order peak (Figure 1a, trace D). Mesostructure retention was corroborated by TEM imaging of various sections of the material, which showed nanoparticles inside the mesopores (Figure 2e). The average sizes of the pores and the nanoparticles were estimated from the TEM image analysis to be 21 and 7 nm, respectively. The material was further characterized by nitrogen physisorption, which showed a type-IV nitrogen sorption isotherm (Figure 4b, trace A) with a specific surface area of 171.5 m^2/g and a pore size distribution centered around 24 nm (see Figure 4b inset, trace A). XRD analysis of the material showed sharp reflections characteristic of highly crystalline Nb_2O_5 (PDF no. 1007-433) as well as broad peaks corresponding to Pt nanoparticles (PDF no. 812-9818) (Figure 3c). The average particle sizes of the Nb_2O_5 and Pt crystallites calculated using the Debye−Scherer formula were 30 ± 4 and 10 ± 2 nm, respectively, in agreement with TEM image analysis. Interestingly, no evidence of Pb (as either Pb nanoparticles or the PtPb intermetallic phase) was found in the XRD analysis, as would be expected for the 1:1 molar ratio of Pt and Pb, when the material was heated to 700 °C. However, EDAX analysis of the material did show a 1:1 ratio of Pt and Pb, and XPS surface analysis confirmed the presence of Pb (Figures S5 and S6, respectively, in the Supporting Information). This indicates that Pb is still contained in the composite but perhaps in a dispersed and disordered form. For an aqueous solution containing 0.5 M FA and 0.1 M H_2SO_4, CCM-Nb_2O_5-C-Pt-Pb with a total Pt−Pb loading of 5 wt % exhibited an onset potential of −0.177 V and a mass activity of 0.149 mA/μg (Figure S7 in the Supporting Information). The more negative onset potential and much higher mass activity (an order of magnitude) for CCM-Nb_2O_5-C-Pt-Pb compared with CCM-Nb_2O_5-C-Pt (Table 1) suggest that Pb reacted with Pt.

To obtain the NbO_2 phase of the oxide material, we reduced CCM-Nb_2O_5-C-Pt-Pb under forming gas at 875 °C for 2 h to produce nanoparticles supported on highly crystalline mesoporous NbO_2 (CCM-NbO_2-C-Pt-Pb). As expected, the order of the parent mesostructured material was not preserved, but the resulting material was still mesoporous. This was supported by nitrogen physisorption measurements showing a type-IV nitrogen sorption isotherm (Figure 4b, trace B) with a specific surface area of 175.2 m^2/g and a slightly broader pore size distribution than for CCM-Nb_2O_5-C-Pt-Pb, centered around 22 nm (see Figure 4b inset, trace B). TEM images of this material showed nanoparticles with an average size of 7 nm well-dispersed in a porous matrix (Figure 2f), very similar to the material without lead. XRD analysis of the material showed the sharp reflections characteristic of highly crystalline NbO_2 (PDF no. 04-005-4298) as well as broader peaks corresponding to Pt nanoparticles (PDF no. 812-9818) (Figure 3d). The average particle sizes of the NbO_2 and Pt crystallites calculated using the Debye-Scherer formula were 80 ± 4 and 10 ± 2 nm, similar to the case without lead.

Trace C in Figure 1b shows the rotating-disk-electrode voltammogram for FA oxidation using CCM-NbO_2-C-Pt-Pb. For an aqueous solution containing 0.5 M FA and 0.1 M H_2SO_4, CCM-NbO_2-C-Pt-Pb with a total Pt−Pb loading of 5 wt % exhibited an onset potential of −0.25 V and a mass activity of 3.3 mA/μg. This result indicates an onset potential that is 60 mV less positive and a mass activity that is 4 times higher than the best reported values for PtPb intermetallic nanoparticles supported on a conducting carbon support, Vulcan-XC-72R[39] (see Figure S8 in the Supporting Information for a comparison of results for these two systems as well as for Pt nanoparticles on Vulcan and Pt−Ru nanoparticles on Vulcan). Additionally, CO stripping voltammograms of CCM-NbO_2-C-Pt-Pb showed very little change between runs after and before CO exposure (Figure S9 in the Supporting Information). Mass activities and onset potentials obtained for FA oxidation using higher loadings of Pt and Pb are presented in Table 1. In all cases, the results are much better than for Pt nanoparticles without Pb supported on conducting carbon (compare with Figure S8). The mass activities decreased with increasing metal loading, which we attribute to the decreased surface area of accessible electrocatalyst. We also examined the activity of this novel nanostructured electrocatalyst toward methanol oxidation, and the results, while not better, were comparable to those for Pt−Pb and Pt−Ru nanoparticles dispersed on conducting carbon (Figure S10 in the Supporting Information).

In order to show that the presence of Pt is necessary, we also investigated the electrocatalytic behavior of mesoporous Nb_2O_5 and mesoporous NbO_2 without the addition of any other metal. Neither showed any activity toward FA oxidation. Next, we added only the Pb precursor to the one-pot synthesis (without Pt precursor). The resulting as-made material was heat-treated under argon at 700 °C as described above to give a highly crystalline Nb_2O_5 material with expected Pb nanoparticles inside the mesopores (CCM-Nb_2O_5-C-Pb). XRD analysis of this material confirmed the crystalline phase of Nb_2O_5, but no crystalline reflections associated with Pb were identified (Figure S11 in the Supporting Information). In contrast, microprobe analysis clearly showed the presence of Pb. This is consistent with the XRD patterns of the materials that contained both Pt and Pb (CCM-Nb_2O_5-C-Pt-Pb and CCM-NbO_2-C-Pt-Pb), as discussed earlier. CCM-Nb_2O_5-C-Pb showed no electrochemical activity toward the oxidation of FA (Figure S12 in the Supporting Information).

While the role of Pb is not fully understood, its presence does increase the mass activity for FA oxidation by an order of magnitude over similarly prepared materials containing only Pt

(37) Alden, L. R.; Han, D. K.; Matsumoto, F.; Abruna, H. D.; DiSalvo, F. J. *Chem. Mater.* **2006**, *18*, 5591–5596.
(38) Casado-Rivera, E.; Volpe, D. J.; Alden, L.; Lind, C.; Downie, C.; Vazquez-Alvarez, T.; Angelo, A. C. D.; DiSalvo, F. J.; Abruna, H. D. *J. Am. Chem. Soc.* **2004**, *126*, 4043–4049.
(39) Matsumoto, F.; Roychowdhury, C.; DiSalvo, F. J.; Abruna, H. D. *J. Electrochem. Soc.* **2008**, *155*, B148–B154.

nanoparticles as the catalyst. It also shifts the onset potential to more negative values compared with CCM-NbO_2-C-Pt (Table 1). We hypothesize that Pb or a Pb-containing compound may be present on part or all of the surface of the Pt nanoparticles, which results in more favorable electrochemical activity toward FA oxidation. Such nanoparticle architecture consisting of a Pt-rich core and a Ru-rich shell has previously been shown for Pt−Ru nanoparticles,[40] which are known to be a good electrocatalyst for methanol oxidation.[22] It is also possible that some Pb is dissolved in the Pt, since the phase diagram shows that Pb is soluble in Pt in small concentrations (the exact amount has not been determined, but as a reference, the solubility of Sn in Pt is known to be 13 wt %).[41] Such low solubility would not lead to detectable changes in the X-ray diffraction pattern of small nanoparticles.

To understand the role of carbon in this material, we measured the conductivity of the composites using a two-point pellet probe. The measured conductivities of the CCM-NbO_2-C and CCM-Nb_2O_5-C samples were 0.12 and 0.015 S/cm, respectively. We attribute the increase in conductivity of the NbO_2 sample over that of the Nb_2O_5 sample to the contribution of the semiconducting NbO_2.[42] In a final experiment, we removed the 15% in situ-generated carbon remaining in the system for CCM-NbO_2-C-Pt-Pb by calcining the material in air at 550 °C for two hours. This process oxidizes the carbon to carbon dioxide gas and NbO_2 to Nb_2O_5. The resulting material was then reduced back to NbO_2 by heat treatment under forming gas at 875 °C. The resulting material did not show any electrochemical activity toward FA oxidation (Figure S13 in the Supporting Information). It should be noted that in addition to removal of the carbon, several other materials parameters were altered during these two additional steps. One of these is the porosity and high surface area of the material. BET surface area analysis on this material showed that the surface area decreased to 8 m^2/g. The in situ-generated carbon is needed to preserve the high surface area and porosity of the material when Nb_2O_5 is reduced to NbO_2 under forming gas at high temperatures. Other possible changes include modifying the surface of the electrocatalyst nanoparticles (upon heat treatment in air) and creating other polymorphs of the oxide (Figure S14 in the Supporting Information). Therefore, this experiment cannot be easily interpreted, but it suggests that the in situ-generated carbon is important for the preparation of this novel nanostructured electrocatalyst. Long-term durability tests (>1000 h) in real fuel-cell assemblies are necessary to determine the material stability but are well beyond the scope of this study.

Conclusion

In summary, we have developed a one-pot synthesis for making Pt- and Pt−Pb-based nanoparticles incorporated into the mesopores of highly crystalline niobium oxide−carbon composites. This technique utilizes the structure-directing properties of block copolymers, which allow for control over dimensions such as pore size and wall thickness by simply varying the block-copolymer molecular weight or block weight fraction. This one-pot method also has the advantage of making uniformly dispersed nanoparticles, as the confinement of the mesopores prevents particle agglomeration, which is often a considerable challenge in nanoparticle synthesis. The resulting mesostructured material, CCM-NbO_2-C-Pt-Pb, shows very promising electrochemical activity toward FA oxidation. The mass activity is 4 times as high as the best previously reported value for Pt−Pb intermetallic nanoparticles supported on conducting carbon. It is not clear at present whether the increased activity is due to a synergy between the catalyst and the NbO_2 support or only to the conductivity of NbO_2. Indeed, Adzic and collaborators[23] have reported an increase in activity for oxygen reduction by Pt when it is supported on NbO_2. While we do not fully understand the exact role of Pb in this system, its addition increases the mass activity of FA oxidation by an order of magnitude over that for pure Pt nanoparticles on the same oxide support while shifting the onset potential to more negative values. While this material does not fully overcome the issue of carbon degradation, our research does signal forward progress in the quest for alternative materials for use as electrode materials in fuel cells. The facile yet versatile one-pot approach can provide an easy way to test various new mesostructured materials as catalyst supports for use in PEMFCs. Moreover, it may provide access to many different metal alloy or intermetallic nanoparticles to be explored as viable catalysts for PEMFCs on a high-surface-area and highly accessible electrocatalyst support.

Acknowledgment. This work was supported by the Department of Energy (DE-FG02 87ER45298) through the Cornell Center for Materials Research and the Cornell Fuel Cell Institute. It was further supported by the National Science Foundation (DMR-0605856) and grants from General Motors. The Cornell High Energy Synchrotron Source (CHESS) is a national user facility supported by the National Science Foundation and the National Institute of General Medical Sciences. The authors are grateful to Sol M. Gruner and Mark W. Tate of the Physics Department of Cornell University for technical assistance and fruitful discussions on the SAXS measurements. We thank Andrew Burns for help with the graphics and figures.

Supporting Information Available: Complete ref 2 and additional TGA, Raman, EDAX analysis, XPS, rotating-disk-electrode voltammogram, and XRD data (Figures S1−14). This material is available free of charge via the Internet at http://pubs.acs.org.

JA903296R

(40) Sarma, L. S.; Chen, C.-H.; Kumar, S. M. S.; Wang, G.-R.; Yen, S.-C.; Liu, D.-G.; Sheu, H.-S.; Yu, K.-L.; Tang, M.-T.; Lee, J.-F.; Bock, C.; Chen, K.-H.; Hwang, B.-J. *Langmuir* **2007**, *23*, 5802–5809.
(41) Hansen, M.; Anderko, K. *Constitution of Binary Alloys*, 2nd ed.; McGraw-Hill: New York, 1958.
(42) Sakai, Y.; Tsuda, N.; Sakata, T. *J. Phys. Soc. Jpn.* **1984**, *54*, 1514–1518.